Density functional study of surface-supported planar magic Ag nanoclusters

Ya-Ping Chiu,[1,*] Ching-Ming Wei,[2,3] and Chia-Seng Chang[2]
[1]*Department of Physics, National Sun Yat-sen University, Taiwan, Republic of China*
[2]*Institute of Physics, Academia Sinica, Taiwan, Republic of China*
[3]*Institute of Atomic and Molecular Sciences, Academia Sinica, Taiwan, Republic of China*
(Received 4 March 2008; revised manuscript received 30 July 2008; published 4 September 2008; publisher error corrected 5 September 2008)

Experimentally, self-organized Ag planar clusters have been observed on the periodic template found on the Pb quantum islands, which are grown on the Si(111) surface. These planar clusters register a remarkable abundance variation at some specific atomic numbers and possess enhanced stability. They are thus denoted as two-dimensional magic Ag nanoclusters (or nanopucks). In this work, detailed calculations based on *ab initio* density functional theory are made to illuminate how the size and shape effects related to electronic confinement influence the sequence of these two-dimensional Ag nanostructures. The simulation results demonstrate that the evolution of a sequence of planar magic Ag clusters is strongly correlated with their electronic structures. Meanwhile, the role of substrate in the formation of magic Ag clusters is also examined. The symmetry and size of the periodic pattern on the substrate have helped to build up the distinguishable geometric structures in experiment. Further analysis of the related electronic and geometrical properties of these clusters not only explains the occurrence and sequence of the magic numbers but also helps to elucidate the mechanism of their formation.

DOI: 10.1103/PhysRevB.78.115402 PACS number(s): 31.15.E−, 73.22.−f, 61.46.−w, 07.79.Cz

I. INTRODUCTION

The unique properties of atomic clusters have been appreciated owing to the recognition of their physical and chemical phenomena as differing from those of individual atoms, molecules, or bulk materials.[1–9] The interpolation between individual atoms and the bulk material does not always yield the characteristics of a particular cluster. The physicochemical properties of the clusters sometimes change dramatically with the addition or removal of a single atom from a cluster, a fact which influences the applications of the material. Therefore, in recent decades, the characterization and potential applications of clusters have attracted considerable interest.[6–8,17–21]

When the size of a metal cluster is comparable with the wavelength of its Fermi electrons, the growth and stability of the cluster is conceivably influenced by its electronic energy. In particular, for simple metal clusters (*sp*-bonded materials) the electron density can be described in terms of single-particle wave functions on a "jellium" mean-field picture.[10–16] Such a simplification allows parallels to be drawn between atomic cluster physics and nuclear physics.[17,22] When this model is adopted, the size-evolutionary patterns of magic alkali-metal clusters can be constructed. A major breakthrough in metal cluster research was the establishment of a correlation between the mass abundance distributions of simple alkali-metal clusters (Na, K) and their corresponding electronic shell-closing structures.[17] These clusters, frequently observed in mass abundance spectra, are so-called magic clusters. They typically exhibit enhanced stabilities and their physicochemical properties are sensitive to their structure and size. Consequently, efforts have been made to tailor the structure and chemical ordering of these materials.[17–21]

More recently, comprehensive surveys of gas-phase and surface-supported magic clusters have been conducted both experimentally and theoretically.[17–34] However, only a few theoretical studies of two-dimensional (2D) magic clusters,[15,23] unlike three-dimensional (3D) magic clusters,[24–33] have been performed. These studies did predict the existence of 2D magic clusters. Hence, substantial efforts have been made to find such two-dimensional clusters for their controlled application in future nanotechnologies.[19–21]

Silver has a distinct position in the periodic table where it resides next to a transition metal. The band structure of a thin silver film, therefore, has a unique property: electronic configuration from 4 eV below the Fermi level upwards is dominated by the atomic 5*s* orbital as calculated in the Sec. III. This investigation reveals the incipient free-electron-like nature of a silver planar cluster, thus rendering the possibility of their growth in magic forms. Recent experimental discoveries have shown that the pattern found on Pb quantum islands formed above Si(111) surfaces can be used to grow two-dimensional Ag nanoclusters via the self-organizing mechanism.[20,34] Not only did Ag nanopucks on Pb islands exhibit notable planar characteristics, but also the distinct size- and shape-evolutionary features of Ag nanopucks reflect a remarkable distribution of nanopuck intensities. Additionally, these magic planar Ag clusters were found to spontaneously aggregate, independent of the image contrast of Pb islands.[35] Since the image contrast of the superstructure primarily reflects differences in the surface charge modulation on Pb islands,[36] the sequence of magic Ag clusters is not affected by the variance of surface potential of Pb islands. Furthermore, a different substrate, graphite, was also employed to grow Ag clusters. Well-defined two-dimensional hexagonal Ag crystalline structures were developed on a smooth graphite surface even at ~25 K.[35] Based on this experimental evidence, it is suggested that Ag clusters *per se* exhibit an intrinsic 2D property. The need to understand theoretically the origins of their formation and their stable structures has motivated this study.

To understand the inherent properties of Ag nanoclusters, the calculations were systematically made within the framework of free-standing Ag clusters, without reference to the substrate effect first. The energetic optimization of 2D planar Ag clusters in configuration space is thoroughly analyzed based on density functional calculations. Since the electronic energy of a nanocluster can be calculated from first principles, various plausible shapes of a Ag nanocluster can be identified considering their relative stabilities. Such a detailed investigation of the cluster energy along this line proves the presence of a series of magic 2D Ag clusters, and an apparent correlation between the size and shape of these planar clusters is demonstrated. A comparison with the experimental data indicated that these calculations that neglect the substrate offer a good basis for determining the stability of clusters when the number of atoms in the cluster is less than 40. However, although theoretical predictions concerning isolated Ag clusters are in good agreement with experimental measurements, magic clusters with 7, 19, and 37 atoms, arranged in highly symmetrical geometries, were not elucidated in the examination of isolated Ag clusters. Additionally, according to recent simulations,[7,8] the transition of neutral Ag clusters from planar to 3D structures begins with Ag clusters of seven atoms. Since these Ag clusters in experiment are supported on a surface, the lack of a prediction of hexagonal magic Ag clusters and the lack of the expected onset of 3D structures raise a critical question regarding the substrate effect. To understand the role of the substrate in the generation of magic planar Ag clusters in the experiment, the calculations were also performed considering it.

The arrangement of this article is as follows. Section II presents the theoretical method for determining the geometry and electronic structure of a Ag cluster using the density-functional-theory (DFT) calculation. The first part of Sec. III shows the results for the low-energy structures and their relationship to the shapes of the clusters. The second part of this section discusses the cluster's stability and the simulated results are compared to the experimental distribution of mass abundance. Sec. IV addresses the origin of the formation of these 2D magic planar Ag nanoclusters determined from the elucidated geometry, electronic characterization, and substrate effects of Ag nanoclusters, using first-principles calculations. Sec. V summarizes our findings.

II. SIMULATION METHODS

The calculations are performed using the Vienna *Ab initio* Simulation Package (VASP), based on the spin-dependent density functional theory and the projector-augmented wave (PAW) method.[37–39] The generalized gradient correction approximation of Perdew, Burke, and Ernzerhof (PBE) is applied to the exchange correlation energy of the electronic density.[40] The supercell geometry is used to simulate two-dimensional Ag nanoclusters with various sizes and shapes. Each cell encloses a free Ag nanocluster, and is separated from the others by a vacuum region with a width of five Ag layers in z direction, perpendicular to the 2D Ag clusters. Additionally, each Ag nanocluster is held at a distance of approximately 12 Å in x (or y) direction from the adjacent one. The Brillouin-zone summation is approximated and performed using a gamma k-point grid, and the plane-wave energy cutoff is 250 eV. In all of the calculations, all atoms in a Ag nanocluster are fully relaxed in x, y, and z directions. The geometry is optimized until the total energy converges to 1×10^{-5} eV.

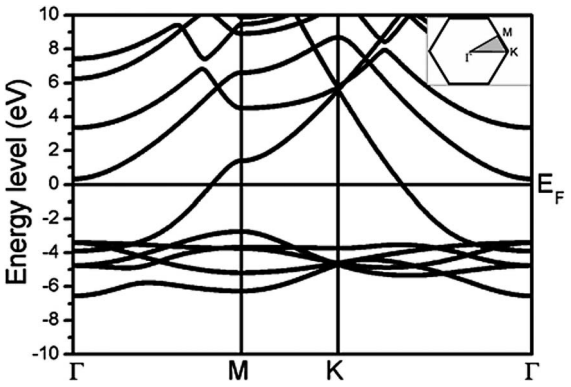

FIG. 1. Band structure of monolayer Ag thin film. *S*-orbital electrons dominate the electronic structure from ~4 eV below the Fermi level upwards.

III. THEORETICAL RESULTS AND DISCUSSION

A. Geometries of 2D Ag_N clusters

Figure 1 presents the band structure of a monolayer Ag crystalline film. The analysis reveals that the calculated electronic states of the Ag thin film near the Fermi level are characterized by a free-electron-like band that is formed from the atomic 5*s* orbital, overlapping (~0.5 eV) with the localized atomic 4*d* orbital at ~4 eV below the Fermi energy. Considering geometric packing in turn, the energetically favorable structures of 3D and 2D clusters are in general of icosahedra and hexagon, respectively. Compared to their relative stabilities of Ag clusters at specific sizes [shown in Fig. 7(b)], Ag clusters are shown to form in planar configurations preferably when the clusters are small. Therefore, in the initial part of this work the energetically favorable structures of planar Ag nanoclusters are investigated.

The possible shapes of Ag nanoclusters of different sizes are determined theoretically by iterations. After fully analyzing these plausible configurations, Table I selects and summarizes the pertinent structural and geometrical properties of the lowest-energy cluster and some representative metastable isomers for Ag_N with N ranging from 3 to 42. The isomers of Ag_N for a given size (N) are ordered according to their relative energetic stability, with the lowest-energy isomer denoted as Type *a*, the next higher energy as Type *b*, and so on. The information given in Table I include the stacking sequence and relative binding energy.

B. Magic 2D Ag_N clusters

The relative binding energy per atom of the lowest-energy planar Ag nanoclusters (E_b) is calculated and plotted in Fig. 2(a) as function of the cluster size. In this figure, the binding energies of these stable structures are compared to those of

TABLE I. Properties of lowest-energy structure and isomers of Ag_N clusters in size range $N=3-42$: total energy difference (ΔE) between possible isomers and the lowest-energy isomer, and the configurations.

N	Type	Stacking	ΔE	N	Type	Stacking	ΔE	N	Type	Stacking	ΔE	N	Type	Stacking	ΔE	N	Type	Stacking	ΔE
3	a	(1,2)	0.0	13	a	(1,2,3,4,3)	0.0	20	a	(4,5,6,5)	0.0	28	a	(4,5,6,7,6)	0.0	35	a	(3,5,6,7,6,5,3)	0.0
4	a	(2,2)	0.0	13	b	(4,5,4)	9.1	20	b	(3,4,5,4,4)	0.5	28	b	(6,7,8,7)	8.6	35	b	(2,5,6,7,6,5,4)	1.3
4	b	(1,2,1)	1.5	13	c	(4,4,5)	31.6	20	c	(3,5,5,4,3)	0.5	28	c	(5,6,6,6,5)	12.3	35	c	(4,5,6,7,7,6)	3.5
5	a	(2,3)	0.0	14	a	(3,4,4,3)	0.0	21	a	(3,4,5,5,4)	0.0	29	a	(2,3,4,5,6,5,4)	0.0	36	a	(3,4,5,6,7,6,5)	0.0
5	b	(2,2,1)	3.6	14	b	(5,5,4)	11.4	21	b	(4,5,6,6)	7.0	29	b	(5,6,7,6,5)	5.3	36	b	(5,6,7,7,6,5)	2.4
6	a	(1,2,3)	0.0	14	c	(2,3,4,5)	29.2	21	c	(3,5,6,7)	18.0	30	a	(4,5,6,6,5,4)	0.0	36	c	(3,5,6,7,6,5,4)	3.0
6	b	(2,2,2)	45.0	15	a	(4,4,4,3)	0.0	22	a	(5,6,6,5)	0.0	30	b	(7,8,8,7)	0.5	37	a	(4,5,6,7,6,5,4)	0.0
7	a	(2,3,2)	0.0	15	b	(2,3,4,4,2)	9.1	22	b	(1,2,3,4,5,4,3)	18.9	30	c	(5,6,7,6,5,1)	1.1	38	a	(3,4,5,6,7,7,6)	0.0
7	b	(3,4)	65.2	15	c	(4,5,6)	44.6	22	c	(5,6,7,4)	19.5	31	a	(3,4,5,5,5,5,4)	0.0	38	b	(5,5,6,7,6,5,4)	6.8
8	a	(1,2,3,2)	0.0	16	a	(4,5,4,3)	0.0	23	a	(4,5,5,5,4)	0.0	31	b	(5,6,7,7,6)	2.8	38	c	(5,6,7,7,7,6)	11.4
8	b	(3,3,2)	0.2	16	b	(2,4,4,4,2)	23.8	23	b	(3,5,6,5,4)	0.9	31	c	(2,3,4,5,6,6,5)	2.9	39	a	(4,6,7,7,6,5,4)	0.0
8	c	(1,2,2,2,1)	105.3	17	a	(1,2,3,4,4,3)	0.0	23	c	(5,6,7,5)	8.0	32	a	(5,6,7,6,5,3)	0.0	39	b	(5,6,7,8,7,6)	2.1
9	a	(2,3,4)	0.0	17	b	(2,4,5,4,2)	17.0	24	a	(4,5,6,5,4)	0.0	32	b	(4,5,6,6,6,5)	8.7	40	a	(4,5,6,7,7,6,5)	0.0
9	b	(4,5)	100.1	17	c	(3,4,4,3,3)	26.3	24	b	(5,6,7,6)	18.0	32	c	(2,5,6,6,6,5,2)	11.8	40	b	(3,4,5,6,7,8,7)	1.8
10	a	(3,4,3)	0.0	18	a	(4,5,5,4)	0.0	25	a	(4,5,6,6,4)	0.0	33	a	(4,5,6,7,6,5)	0.0	41	a	(4,6,7,7,7,6,4)	0.0
10	b	(3,3,4)	52.8	18	b	(3,4,5,6)	1.5	25	b	(5,5,5,5,5)	26.6	33	b	(5,6,7,8,7)	10.6	41	b	(2,4,5,6,7,6,5,4,2)	0.2
11	a	(1,2,3,3,2)	0.0	18	c	(2,4,5,4,3)	1.9	26	a	(4,5,6,6,5)	0.0	33	c	(6,7,7,7,6)	12.0	41	c	(5,6,7,8,8,7)	4.6
11	b	(4,4,3)	114.4	19	a	(3,4,5,4,3)	0.0	26	b	(6,7,7,6)	12.4	34	a	(3,5,6,6,6,5,3)	0.0	42	a	(6,7,8,8,7,6)	0.0
12	a	(2,3,4,3)	0.0	19	b	(3,5,5,5)	3.7	27	a	(3,4,5,6,5,4)	0.0	34	b	(6,7,8,7,6)	2.1	42	b	(5,7,8,7,6,5,4)	3.1
12	b	(4,4,4)	38.8					27	b	(4,5,5,5,4,4)	8.8	34	c	(4,5,6,6,5,4,4)	4.9	42	c	(4,5,6,7,7,7,6)	6.2

geometrically stable hexagons, which are guided with a dashed curve. Most calculated binding energies per atom stay close to this curve except a few smaller clusters. Since a magic cluster reflects the relative stability of a planar Ag cluster with respect to its neighboring sizes, the second derivative $\Delta^2 E_b(N)$ in binding energy, which sensitively captures the difference between the binding energies of adjacent clusters $2E_b(N)-[E_b(N+1)+E_b(N-1)]$ on N [plotted in Fig. 2(b)] clearly yields information on the formation of a magic cluster. The value of this second derivative hence represents the strength of a magic cluster's stability. Local maximum peaks of $\Delta^2 E_b(N)$ are found at $N=6$, 8, 10, 12, 22, 24, 29, and 40, suggesting that the clusters with these values of N are more stable than their neighboring clusters. The calculated major magic numbers are in large consistent with the experimental results.[20] The inconsistency associated with size $N=34$ may be attributable to the substrate effect in the experiments, which has not been considered in the theoretical simulations. Figure 3 depicts the geometric structures of the magic clusters that are most frequently observed in experiments.

IV. MECHANISM OF FORMATION OF 2D AG CLUSTERS

A. Electronic characteristics of 2D Ag clusters

From the above examination, the important question regarding the origin of these 2D Ag clusters should be addressed. Generally speaking, the energy gap between the highest occupied molecular orbital (HOMO) and the lowest unoccupied molecular orbital (LUMO) associated with each cluster ought to provide some indication. A larger HOMO-LUMO energy gap implies a relatively higher stability of the system, and the system is dominated by the electronic effect rather than the geometry of atom packing. The HOMO-LUMO gap of each 2D Ag_N ($N=3-40$) cluster was determined from spin-dependent DFT calculations, and the results are plotted in Fig. 2(c). The HOMO-LUMO gap is higher for Ag_N with $N=6$, 8, 10, 12, 22, 24, and 34. Energy gap near the Fermi level has also been measured experimentally for Ag_{24} and Ag_{34}.[20] From the result shown in Fig. 2(c), it clearly indicates that the mechanism of formation of 2D magic Ag_N with $N=6$, 8, 10, 12, 22, 24, and 34 mainly involves the electronic contribution. However, clusters with 29 and 40 atoms, experimentally identified as magic clusters,[20] do not show the apparent HOMO-LUMO energy gap here. In addition, the HOMO-LUMO gap of Ag clusters generally declines as the cluster size N increases, implying that those larger stable clusters should have some other responsible mechanism than the electronic, and a transition between the dominant factors in the generation of these magic clusters should take place at a certain size.

B. Geometric properties of 2D magic Ag clusters

Geometrical shape is another possible factor contributing to the formation of clusters in magic numbers.[18,24,25] Since the overall shape of the clusters can be deduced from the moments of inertia, detailed inspection of the characteristic reveals the dependence of the geometrical properties of stable cluster configurations on N and elucidates the forma-

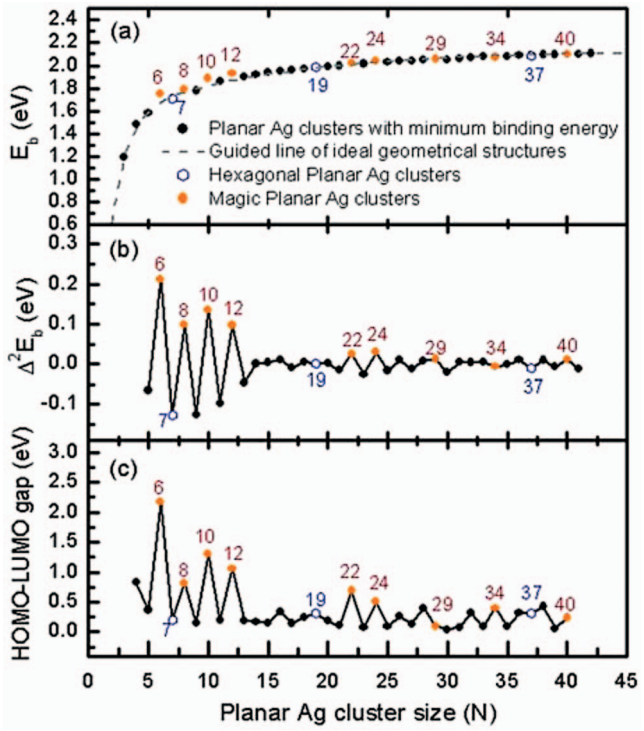

FIG. 2. (Color) (a) Ground-state binding energy per atom as a function of cluster size N. The solid black circles are calculated for the two-dimensional Ag nanoclusters with the lowest energy at a specific size; the orange circles refer to magic 2D nanoclusters, and the open blue hexagons refer to 2D hexagonal magic nanoclusters. (b) Stability based on the second derivatives of total energy versus number of atoms in planar nanoclusters. (c) HOMO-LUMO gap against cluster size N.

tion of these magic clusters due to the geometrical effect. The evolution of the geometrical properties of 2D Ag clusters is further examined by examining their moments of inertia. Based on this definition, the normalized moments of inertia, I, is given by

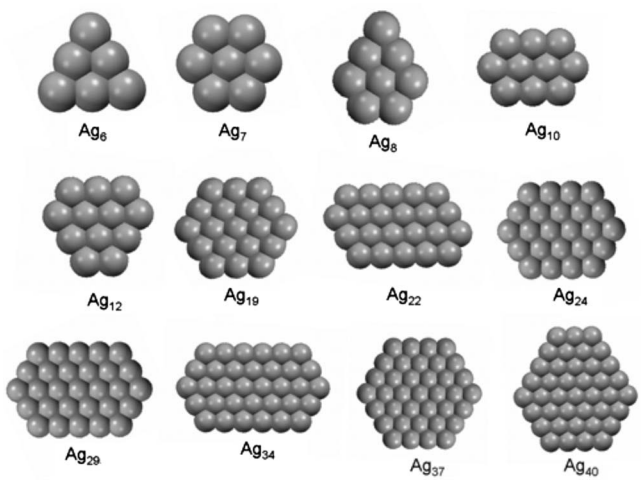

FIG. 3. Geometries of lowest-energy structures or frequently observed for Ag clusters in experiment. The labels indicate the cluster size.

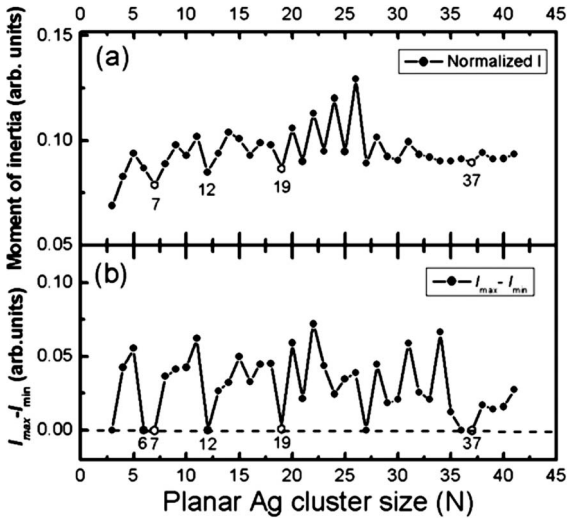

FIG. 4. Moments of inertia versus clusters size N: (a) normalized moments of inertia and (b) difference between normalized largest and smallest principal moments of inertia as a function of cluster size.

$$I = \frac{1}{N^2}\sum_{i=1}^{N} (\vec{R_i} - \overrightarrow{R_{c.m.}})^2,$$

where $\vec{R_i}$ refers to each Ag atom position and $(\vec{R_i} - \overrightarrow{R_{c.m.}})$ is the distance of each atom from the center of mass (in units of Å). The factor $1/N^2$ in the equation is adopted to normalize the moments of inertia. Figure 4(a) plots the normalized moments of inertia of various Ag clusters. The moments of inertia of the magic Ag_N clusters are minimal for $N=7$, 12, 19, and 37. Among these clusters, those with 7, 19, and 37 atoms were also frequently observed in experiments and displayed remarkable stability. It suggests that the magic nature of the clusters with $N=7$, 19, and 37 originates mainly from the ideal geometric packing.

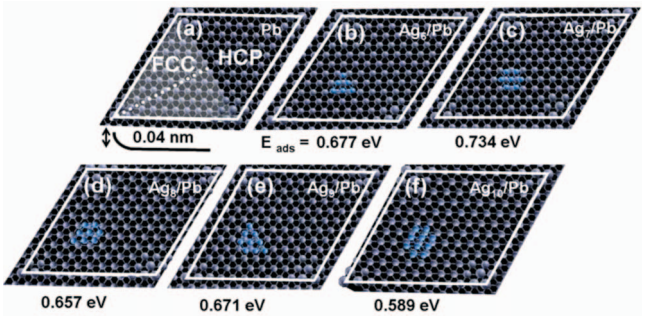

FIG. 5. (Color) Sketch of generation of Moiré pattern in unit cell of Pb quantum island surfaces. Fcc region represents the zone of relative stability for the initial growth of Ag on Pb surfaces. Clean simulated Pb surface (a) and cross-sectional profile for Ag cluster nucleated on simulated fcc region of Pb surfaces are also illustrated below (a). (b)–(f) are represented geometrical configurations for planar Ag_N clusters ($N=6-10$) on simulated substrate. The numbers below (b)–(f) indicate the energies of adsorption per atom for Ag clusters.

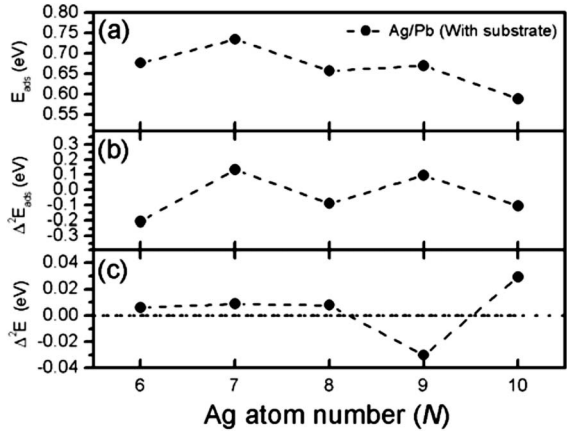

FIG. 6. (a) Ag clusters that gain extra energy per atom as they are adsorbed on Pb surfaces. (b) Second derivatives $\Delta^2 E_{ads}$ of adsorbing energy. (c) Second derivatives $\Delta^2 E$ of energy for the complete system of planar Ag clusters grown on Pb surfaces.

Decomposing the cluster on the basis of moments of inertia can help further elucidate the geometry of clusters. Figure 4(b) plots the dependence of the difference between the maximum and minimum components of the normalized principal moments of inertia and the cluster size N. The result in Fig. 4(b) reveals again that magic clusters with 7, 19, and 37 atoms are arranged in highly symmetrical geometries.

C. Substrate effect on the formation of 2D magic Ag clusters

Since the clusters with 7, 19, and 37 atoms stacking are elucidated principally from geometrically symmetrical packing, whether the substrate have effect on the formation of these geometrically stable clusters to be abundant by experimental observations is desired to know.

Figure 5(a) depicts a unit cell of the Moiré pattern observed on a Pb quantum island grown on the Si(111) substrate.[20,34,36,41] The gray fcc region represents the effective area for the initial growth of Ag clusters on Pb surfaces. In the calculation which considers the substrate effect, the corner site of the unit cell is slightly higher than the central area with a fixed height of 0.04 nm [indicated in Fig. 5(a)].[41] The optimum position and orientation for a cluster on the topmost Pb layer were determined from varying its degrees of freedom. As Ag clusters are formed on the layout surface, two-dimensional Ag_N clusters (N=6–10) are fully relaxed in x, y, and z directions. Figures 5(b)–5(f) present the stable arrangements of Ag clusters with N atoms (N=6–10) grown on Pb islands. The energy for the adsorption of Ag clusters on the quantum Pb island surfaces is evaluated by

$$E_{\mathrm{ads}}(N) = -\frac{1}{N}[E_{\mathrm{Ag/Pb}} - (N \times E_{\mathrm{Ag}} + E_{\mathrm{Pb}})],$$

where N denotes the number of atoms in a specific planar Ag cluster on the Pb surface, and the total energies of the adsorbate-substrate system, the clean Pb surface, and the energy per atom of a free planar Ag cluster are represented by $E_{\mathrm{Ag/Pb}}, E_{\mathrm{Pb}}$, and E_{Ag}, respectively. The adsorption energy, $E_{\mathrm{ads}}(N)$, is the energy that a free Ag atom of a cluster gains by being adsorbed on the surface. Accordingly, it is defined such that a positive number corresponds to exothermic (stable) adsorption with respect to a free Ag atom and a negative number indicates endothermic (unstable) adsorption. Figure 6(a) presents the extra extrinsically gained energy for Ag clusters with different sizes on the Pb surface based on the above definition. Furthermore, in order to extract the relative stability, the second derivative $\Delta^2 E_{\mathrm{ads}}(N)$ [Fig. 6(b)] is considered again from the total binding energy per atom for planar Ag clusters that are grown on Pb quantum islands. Figure 2(b) reveals that the intrinsic Ag cluster

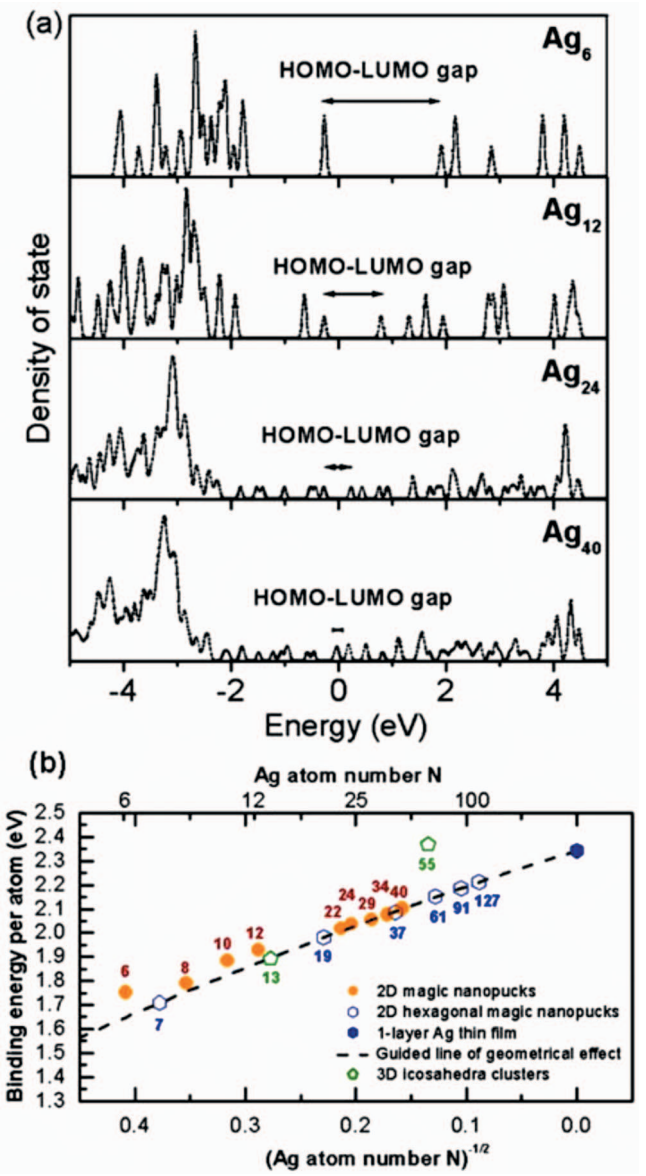

FIG. 7. (Color) (a) The electronic density of states (DOS) of planar Ag nanoclusters, Ag_N, with N=6, 12, 24, and 40. The width of the smearing in 0.05 eV is used. (b) Binding energy per atom against inverse of square root of number of Ag atoms. The dotted line is fitted through the geometrical hexagonal structures. The magic clusters formed in ideal geometrical shapes are represented by open blue hexagons, and others are represented by orange solid circles. The relative stabilities of 3D icosahedra and 2D hexagon clusters are also shown for comparison.

of eight atoms with a proper arrangement are more stable than Ag_7 and Ag_9 without deliberation of the substrate effect. However, when the substrate effect is considered, as in Fig. 6(b), planar Ag_7 and Ag_9 clusters acquire extra energy and their formations are consequently stabilized. When $E_b(N)$ for free Ag clusters weighs in $E_{ads}(N)$ for planar Ag clusters with seven and eight atoms on Pb surfaces, their relative stabilities exceed that of Ag_9, suggesting that planar Ag_7 and Ag_8 clusters have higher binding energies per atom as shown in Fig. 6(c). This analysis demonstrates that Ag_7 and Ag_8 clusters should be more prevalent as the substrate effect is taken into account, corresponding well with the experimental findings.[20]

The transition between the dominant factors in the formation of these magic Ag nanoclusters was elucidated by examining the electronic density of states (DOS) of numerous illustrative Ag clusters—Ag_6, Ag_{12}, Ag_{24}, and Ag_{40}. As displayed in Fig. 7(a), the DOS for Ag_6 are relatively discrete, and the HOMO-LUMO gap is large. As the cluster size increases further, its DOS becomes dense and broadened. The HOMO-LUMO energy gap thus declines notably. This behavior also supports the previous statement that the electronic characteristic became trivial as the cluster grew to a certain size. The binding energy per atom [Fig. 7(b)] is plotted against the reciprocal of the square root of N, enabling the planar cluster energy to be determined from the curvature of the cluster surface. Hence, the dotted line in Fig. 7(b) is associated with the planar hexagonal Ag nanoclusters formed in ideal geometrical shapes. The line in Fig. 7(b) thus divides the clusters into two groups—stable and unstable. Apparently, the corresponding binding energies of small clusters exceed those of hexagonal clusters. They are thus stable and frequently observed with experiment.[20] As the cluster grows, its binding energy slowly approaches the dotted line, which connects all the Ag clusters in the hexagonal shape. It suggests that the transition from the electronic to geometric indeed smoothly occurs in the mechanism dictating the growth evolution of the magic Ag nanoclusters.

V. CONCLUSIONS

We have performed systematic calculations and simulations to obtain the magic sizes and their corresponding equilibrium structures for two-dimensional Ag nanoclusters (Ag_N, $N=3-42$) grown on the Pb surface. The dependences of binding energy, second derivative of binding energy $\Delta^2 E_b$, HOMO-LUMO energy gap, and moments of inertia on the cluster size N are analyzed and considered. Both the large HOMO-LUMO energy gap and highly symmetric geometry are identified as the essential factors for the energetically favorable structures. However, the HOMO-LUMO gap markedly decreases as the Ag nanocluster grows to a particular size, implying that the geometrical effect develops with the cluster's size while the electronic effect subsides. The calculated electronic and geometrical structures of these magic clusters are well correlated with the experimental findings. The substrate plays a crucial role on the formation of the hexagonal magic Ag clusters and the postponing of the onset of three-dimensional Ag clusters in the experiment even for Ag clusters of 127 atoms.

ACKNOWLEDGMENTS

The authors would like to thank the financial support of this study by the National Science Council of Taiwan, Republic of China under the Contract No. NSC 95-2112-M-110-024-MY3.

*Corresponding author

[1] E. Kaxiras, *Atomic and Electronic Strcuture of Solids* (Cambridge University Press, Cambridge, England, 2003).
[2] *Metal Clusters*, edited by Martin Moskovits (Wiley, New York, 1986).
[3] *Metal Clusters*, edited by W. Ekardt (Wiley, New York, 1999).
[4] *Metal Clusters at Surfaces, Structure, Quantum Properties, Physical Chemistry*, Springer Series in Cluster Physics, edited by K.-H. Meiwes-Broer (Springer, Berlin, 1999).
[5] Matthias Brack, Rev. Mod. Phys. **65**, 677 (1993).
[6] M. Pereiro, D. Baldomir, and J. E. Arias, Phys. Rev. A **75**, 063204 (2007).
[7] Eva M. Fernández, José M. Soler, Ignacio L. Garzón, and Luis C. Balbás, Phys. Rev. B **70**, 165403 (2004).
[8] M. Pereiro and D. Baldomir, Phys. Rev. A **75**, 033202 (2007).
[9] M. Payami, Phys. Rev. B **73**, 113106 (2006).
[10] N. D. Lang and A. R. Williams, Phys. Rev. B **18**, 616 (1978).
[11] N. D. Lang and W. Kohn, Phys. Rev. B **1**, 4555 (1970).
[12] N. D. Lang and W. Kohn, Phys. Rev. B **3**, 1215 (1971).
[13] W. Ekardt, Phys. Rev. B **29**, 1558 (1984).
[14] W. Ekardt, Phys. Rev. Lett. **52**, 1925 (1984).
[15] C. Kohl, B. Montag, and P.-G. Reinhard, Z. Phys. D: At., Mol. Clusters **38**, 81 (1996).
[16] René Fournier, J. Chem. Phys. **115**, 2165 (2001).
[17] W. D. Knight, K. Clemenger, W. A. de Heer, W. A. Saunders, M. Y. Chou, and M. L. Cohen, Phys. Rev. Lett. **52**, 2141 (1984).
[18] O. Echt, K. Sattler, and E. Recknagel, Phys. Rev. Lett. **47**, 1121 (1981).
[19] M. Y. Lai and Y. L. Wang, Phys. Rev. Lett. **81**, 164 (1998).
[20] Ya-Ping Chiu, Li-Wei Huang, Ching-Ming Wei, Chia-Seng Chang, and Tien-Tzou Tsong, Phys. Rev. Lett. **97**, 165504 (2006).
[21] D. Torrent, J. Sánchez-Dehesa, and F. Cervera, Phys. Rev. B **75**, 241404(R) (2007).
[22] B. K. Rao, S. N. Khanna, and P. Jena, J. Cluster Sci. **10**, 477 (1999).
[23] S. K. Nayak, P. Jena, V. S. Stepanyuk, W. Hergert, and K. Wildberger, Phys. Rev. B **56**, 6952 (1997).
[24] I. A. Harris, R. S. Kidwell, and J. A. Northby, Phys. Rev. Lett. **53**, 2390 (1984).
[25] K. Manninen, J. Akola, and M. Manninen, Phys. Rev. B **68**, 235412 (2003).
[26] A. Koshelev, A. Shutovich, I. A. Solovyov, A. V. Solovyov, and W. Greiner, Phys. Rev. Lett. **90**, 053401 (2003).

[27] Francesca Baletto and Riccardo Ferrando, Rev. Mod. Phys. **77**, 371 (2005).
[28] H. Häkkinen and M. Manninen, Phys. Rev. Lett. **76**, 1599 (1996).
[29] Andrey Lyalin, Ilia A. Solov'yov, Andrey V. Solov'yov, and Walter Greiner, Phys. Rev. A **67**, 063203 (2003).
[30] H. Häkkinen, M. Moseler, O. Kostko, N. Morgner, M. A. Hoffmann, and B. Issendorff, Phys. Rev. Lett. **93**, 093401 (2004).
[31] B. K. Rao, S. N. Khanna, and P. Jena, Phys. Rev. B **36**, 953 (1987).
[32] Jaakko. Akola, Matti Manninen, Hannu Häkkinen, Uzi Landman, Xi Li, and Lai-Sheng Wang, Phys. Rev. B **62**, 13216 (2000).
[33] Baolin Wang, Jijun Zhao, Xiaoshuang Chen, Daning Shi, and Guanghou Wang, Phys. Rev. A **71**, 033201 (2005).
[34] H. Y. Lin, Y. P. Chiu, L. W. Huang, Y. W. Chen, T. Y. Fu, C. S. Chang, and Tien T. Tsong, Phys. Rev. Lett. **94**, 136101 (2005).
[35] See EPAPS Document No. E-PRBMDO-78-015835 for experimental findings for these Ag clusters grown on different supports. For more information on EPAPS, see http://www.aip.org/pubservs/epaps.html.
[36] W. B. Jian, W. B. Su, C. S. Chang, and T. T. Tsong, Phys. Rev. Lett. **90**, 196603 (2003).
[37] J. P. Perdew, K. Burke, and M. Ernzerhof, Phys. Rev. Lett. **77**, 3865 (1996).
[38] W. Kohn and L. J. Sham, Phys. Rev. **140**, A1133 (1965).
[39] G. Kresse and J. Hafner, Phys. Rev. B **47**, 558 (1993); **49**, 14251 (1994); G. Kresse and J. Furthmuller, *ibid.* **54**, 11169 (1996); Comput. Mater. Sci. **6**, 15 (1996).
[40] G. Kresse and D. Joubert, Phys. Rev. B **59**, 1758 (1999).
[41] S. M. Lu, M. C. Yang, W. B. Su, C. L. Jiang, T. Hsu, C. S. Chang, and Tien T. Tsong, Phys. Rev. B **75**, 113402 (2007).